Avicenna Journal of Phytomedicine (AJP)

Original Research Article

Biological effects of green-synthesized zinc oxide nanoparticles with *Portulaca oleracea* extract on AGS gastric cancer cells: Anti-angiogenic, antioxidant, and apoptotic effects

Mohammadreza Pourmohammad[1], Fatemeh Faravani[2], Jina Khayatzadeh[3,*], Saeedeh Zafar Balanjad[4]

[1]*Department of Parasitology and Mycology, School of Allied Medical Sciences, Ilam University of Medical Sciences, Ilam, Iran*
[2]*Department of Biology, Ma.C., Islamic Azad University, Mashhad, Iran*
[3]*Department of Biology, Ma.C., Islamic Azad University, Mashhad, Iran*
[4]*Department of Biology, Ma.C., Islamic Azad University, Mashhad, Iran*

Article history:
Received: Jul 29, 2025
Received in revised form: Jul 12, 2026
Accepted: Jul 28, 2026
Epub ahead of print

**** Corresponding Authors:***
Jkhayatzadeh@iau.ac.ir

Keywords:
ZnO NPs
Portulaca oleracea
Apoptosis
AGS cells
Angiogenesis
Antioxidant activity

Abstract

Objective: This study investigated the therapeutic potential of green-synthesized zinc oxide nanoparticles (ZnO NPs) derived from aqueous extract of *Portulaca oleracea* aerial parts as a novel, biocompatible agent against gastric cancer. Given the limitations of conventional treatments, including drug resistance and systemic toxicity, targeted anticancer strategies are urgently needed.

Materials and Methods: The synthesized ZnO NPs were characterized using TEM, FESEM, AFM, and XRD. Their cytotoxic effects were evaluated in AGS human gastric cancer cells and normal HEK-293 cells using the MTT assay. Apoptotic mechanisms were investigated by Annexin V-PI staining, DAPI staining, and gene expression analysis of *Bax*, *P53*, *Caspase-3*, *Caspase-9*, and *Bcl-2*. The anti-angiogenic activity of the NPs was assessed using the chorioallantoic membrane (CAM) assay.

Results: The ZnO NPs exhibited significant concentration- and time-dependent cytotoxicity against AGS cells, while causing minimal toxicity in HEK-293 cells. The antioxidant assay revealed significant concentration- and time-dependent antioxidant activity, with enhanced effects following prolonged exposure. Apoptosis was identified as the primary mechanism of cell death, as demonstrated by morphological alterations, increased apoptotic cell populations, and upregulation of pro-apoptotic genes, accompanied by downregulation of the anti-apoptotic *Bcl-2* gene. In the CAM model, the NPs showed potent, dose-dependent anti-angiogenic activity by reducing vascular branching and vessel length and adversely affecting embryo development.

Conclusion: Green-synthesized *P. oleracea*-derived ZnO NPs exerted anticancer effects through the combined induction of apoptosis, inhibition of angiogenesis, and antioxidant activity. These findings support their potential as a promising complementary nanotherapeutic strategy for gastric cancer treatment.

Please cite this paper as:
Pourmohammad M, Faravani F, Khayatzadeh J, Zafar Balanjad S. Biological effects of green-synthesized zinc oxide nanoparticles with Portulaca oleracea extract on AGS gastric cancer cells: Anti-angiogenic, antioxidant, and apoptotic effects. Avicenna J Phytomed, 2026

Introduction

Gastric cancer remains a major global health concern, being a leading cause of cancer-related deaths despite diagnostic and treatment advancements (Sung et al. 2021). Conventional treatments like chemotherapy and radiation often face challenges such as severe side effects, drug resistance, and low cancer cell specificity (Haider et al. 2020). This highlights an urgent need for novel, more effective, and less toxic anticancer agents that specifically target malignant cells and overcome current therapeutic limitations.

Nanotechnology offers a groundbreaking approach in biomedical applications, particularly for cancer treatment (Acebes-Fernández et al. 2020). Nanoparticles (NPs) leverage their unique physicochemical properties—small size, high surface-to-volume ratio, and tunable surface chemistry—for targeted drug delivery, diagnostics, and therapeutics (Wang et al. 2009). Zinc oxide nanoparticles (ZnO-NPs) are of particular interest due to their established anticancer, antibacterial, and antioxidant properties (Mishra et al. 2017; Li et al. 2021). Their ability to modulate oxidative stress, disrupt cellular pathways, and trigger apoptosis in various cancer cell lines makes them a promising focus for anticancer research (Ma and Yang 2016).

However, traditional chemical and physical synthesis methods often involve harsh chemicals and high energy consumption, raising environmental and toxicity concerns (Singh et al. 2023). Green synthesis, using natural extracts from plants, fungi, or bacteria, has emerged as a sustainable and cost-effective alternative, producing biocompatible nanoparticles without toxic byproducts (Rauf et al. 2025). *Portulaca oleracea* (purslane), a widely available medicinal plant, is rich in bioactive compounds like antioxidants, vitamins, and fatty acids, all with documented therapeutic effects (Golzar et al. 2023; Xia et al. 2024). Its rich phytochemical profile makes it an excellent candidate for green synthesis, potentially enhancing nanoparticle biological efficacy (Eker et al. 2025).

This study investigates the biological effects of ZnO-NPs, green-synthesized using *P. oleracea* extract, on AGS cells (human gastric adenocarcinoma). Our objective is to evaluate their impact on key cancer hallmarks: angiogenesis (new blood vessel formation), antioxidant activity (regulation of cellular oxidative stress), and apoptosis (programmed cell death). By exploring these diverse effects, this research aims to elucidate the therapeutic potential of *P. oleracea*-mediated green-synthesized ZnO-NPs as a promising agent for gastric cancer treatment.

Materials and Methods

This project was conducted at the Department of Biology, Faculty of Sciences, Islamic Azad University, Mashhad Branch, with ethical approval (Code: IR.IAU.MSHD.REC.1402.159) from the Ethics Committee of Islamic Azad University, Mashhad Medical Sciences Branch. The study was approved by the Young Researchers and Elite Club of Khorasan Razavi Province and performed in the first half of 2023.

Aqueous extract preparation

Portulaca oleracea aerial parts (herbarium code 10340) were collected from Ferdows County, South Khorasan Province, Iran. The aerial parts were air-dried and finely powdered. Twenty grams of powder were steeped in 200 mL distilled water for 72 hr at room temperature with occasional shaking. The extract was then filtered (Whatman No. 42), and the solvent was evaporated at 100°C for one hour. The concentrated extract was stored at 4°C (Khan et al. 2022).

Green synthesis of ZnO-NPs

For ZnO-NPs synthesis, 3.6 g zinc acetate powder was dissolved in 100 mL distilled water. Concurrently, 25 mL of *P.*

oleracea extract was stirred at 35°C. Four milliliters (mL) of zinc acetate solution was added dropwise to the extract until a color change occurred. The mixture was then centrifuged (2000 RPM, 20 min), the supernatant was discarded, and precipitated NPs were re-dispersed in distilled water. This purification was repeated twice. Finally, the suspension was ultrasonicated for 10 min before biological assays (Sirelkhatim et al. 2015).

Characterization of green-synthesized ZnO-NPs

Green-synthesized ZnO-NPs were characterized for morphology, size, and optical properties at Bu-Ali Research Institute, Mashhad, Iran, using methods such as X-ray Diffraction (XRD), Transmission Electron Microscopy (TEM), Dynamic Light Scattering (DLS), Fourier-transform infrared (FTIR) spectroscopy, and Field Emission Scanning Electron Microscopy (FESEM). The results confirmed the successful synthesis of the nanoparticles, with 99.3% of the particles being in the nanoscale range and having an average size of 44.6 nm.

Cell culture

AGS cells and HEK-293 human embryonic kidney fibroblast cells (Ferdowsi University of Mashhad Cell Bank, Mashhad, Iran) were cultured in RPMI-1640 and Dulbecco's Modified Eagle Medium (DMEM), respectively, supplemented with 10% fetal bovine serum (FBS) and 1% penicillin/streptomycin. Cells were maintained at 37°C in a humidified 5% CO2 incubator. For subculturing, cells were detached with 0.25% trypsin-EDTA, counted with Trypan Blue, and seeded at 437 cells/well in 96-well plates. This specific low density was intentionally chosen to ensure the cells remained in the exponential growth phase, which allowed for a direct and accurate assessment of the initial cytotoxic effects of the NPs without confounding factors such as contact inhibition. The cells were incubated for 24 hr prior to experiments (Weiskirchen et al. 2023).

Cytotoxicity assay

Cytotoxic effects of ZnO-NPs were assessed using the MTT assay. AGS and HEK-293 cells were seeded in 96-well plates. After 24 hr, fresh media containing ZnO-NPs at the following concentrations (1, 2, 4, 6, 10, 15, and 20 µg/mL) were added, and the cells were subsequently incubated for 24, 48, and 72 hr. Supernatants from 48- and 72-hr time points were collected for antioxidant testing. After incubation, 15 µL MTT solution (5 mg/mL) was added for 3 hr, followed by 100 µL Dimethyl sulfoxide (DMSO) to dissolve formazan crystals. Absorbance was read at 570 nm. Cell viability was calculated as (Mean absorbance of treated wells / Mean absorbance of control wells) × 100 (Wiertelak-Makała et al. 2023).

Assessment of antioxidant activity

Total antioxidant status (TAS) of ZnO-NPs was determined using a Naxifer™ kit (Pars Azmoon, Tehran, Iran) based on the ferric reducing antioxidant power (FRAP) assay. Five microliters of standards or nanoparticle-treated cell culture supernatants (from cytotoxicity assay) were added to a 96-well plate, followed by 250 µL working solution. Absorbance was measured at 593 nm after 15 min. Total antioxidant capacity was quantified using a standard curve and expressed in mmol Fe^{2+}/L.

Apoptosis assay (Annexin V/PI Staining)

Apoptosis induction in AGS and HEK-293 cells was assessed using the Annexin V-FITC Apoptosis Detection Kit (Pars Azmoon, Tehran, Iran). Briefly, 1-5 × 10^5 cells were centrifuged (1500 rpm, 5 min), washed with PBS, and resuspended in 500 µL 1X binding buffer. Two microliters Annexin V-FITC was added (10-15 min, room temperature, dark), followed by 1-2 µL Propidium Iodide (PI) solution (5-10

min, room temperature, dark) before flow cytometry analysis (Alshiraihi and Kato 2023).

Nuclear staining (DAPI)

DAPI staining (1-2 µg/mL) was used to assess nuclear morphology in AGS cells treated at IC50 concentrations for 48 and 72 hr, alongside untreated controls. After incubation (15 min), DAPI was removed, and 1 mL methanol added for cell sedimentation. Nuclear morphology was studied under a fluorescence microscope in the dark (Hosseinpour et al. 2025).

Gene expression analysis

Real-time quantitative PCR (RT-qPCR) was employed to quantify the expression of key apoptosis-related genes, namely *Bax*, *P53*, *Caspase 3*, *Caspase 9*, and *Bcl-2*. Total RNA was isolated from both untreated control and treated AGS cells (at IC50 concentrations of 24.84 µg/mL for 48 hr and 16.88 µg/mL for 72 hr) using a commercially available RNA extraction kit. The quality and concentration of the RNA were assessed by spectrophotometry at 260 nm and 280 nm. Following reverse transcription into cDNA, gene expression was quantified using SYBR Green Master Mix, with GAPDH serving as the internal reference gene (Table 1). The thermal cycling conditions were initiated with a denaturation step at 95°C for 2 min, followed by 40 cycles of denaturation (95°C for 15 sec), annealing (30 sec at gene-specific temperatures of 59°C for *Bax*, 60°C for *P53*, 58°C for *Caspase 3*, 57°C for *Caspase 9*, and 56°C for *Bcl-2*), and extension (72°C for 30 sec). The process concluded with a final extension at 72°C for 5 min. To ensure the accuracy and reproducibility of the results, all RT-qPCR reactions were carried out in technical triplicates, with biological replicates also being performed. The average values derived from these replicates were used for subsequent gene expression analysis. This methodological approach was meticulously implemented to conform to established scientific standards, thereby strengthening the reliability of our quantitative findings (Bustin et al. 2009).

Table 1. Primer sequences and gene details for quantitative real-time pcr analysis

Gene Symbol	Gene Name	Primers (5′ → 3′)
GAPDH	Glyceraldehyde-3-phosphate dehydrogenase	Forward: 5'-TGGAAGGACTCATGACCACAGT-3' Reverse: 5'-TTCCCGTTCAGCTCAGGGAT-3'
Caspase3	Cysteine-aspartic acid protease 3	Forward: 5'-CAAACTGGTGCTCAAGGCCC-3' Reverse: 5'-GAAGTCCAATGTCCAGCCCA-3'
Caspase9	Cysteine-aspartic acid protease 9	Forward: 5'-TCCTACTCTACTTTCCCAGGTTT-3' Reverse: 5'-AAAGCAACCAGGCATCTGTT-3'
Bax	*Bcl-2*-associated X protein	Forward: 5'-AACAGCTTTGAGGTGCGTGT-3' Reverse: 5'-GTTGGGCAGTGCTCGCTT-3'
P53	Tumor suppressor protein	Forward: 5'-TGGAATTGATGCGTGATGTTTCT-3' Reverse: 5'-ACTTCTACAACGATCCCCTCTG-3'
Bcl-2	B-cell lymphoma 2	Forward: 5'-TGAACTGGGGGAGGATTGT-3' Reverse: 5'-AAATCAAACAGAGGCCGCA-3'

Angiogenesis assay (Chorioallantoic Membrane test)

The chorioallantoic membrane (CAM) assay evaluated the angiogenic effects of ZnO-NPs. Fertilized chicken eggs were incubated for 8 days. On day 8, a window was created in the eggshell, and a sterile sponge was placed on the CAM. Sponges were treated with 10 µL of green-synthesized ZnO-NPs (400, 500, 600, and 700 µg/mL), or normal saline (vehicle control), or left untreated (laboratory control). Windows were sealed, and eggs re-incubated. On day 12, angiogenic changes were assessed, and the vascular network was photographed using a stereomicroscope to quantify angiogenic response (Menemenli et al. 2025).

Statistical analysis

All statistical analyses were performed using SPSS software (v. 26) and GraphPad Prism 9. Data normality was assessed, and differences among groups were analyzed using one-way analysis of variance (ANOVA). Results are reported as mean ± standard error of the mean (SEM) from at least three independent replicates. A p-value <0.05 was considered statistically significant.

Results

Characterization of green-synthesized ZnO-NPs

Green-synthesized ZnO-NPs, derived from *P. oleracea* extract, were comprehensively characterized using TEM, FESEM, and AFM (Figure 1). Analysis showed an average particle size of 44.6 nm and a high nanoparticle participation rate of 99.3%, confirming efficient synthesis. AFM (Figure 1a) revealed distinct, elongated nanoscale structures. The histogram from AFM (Figure 1b) showed 66.9% of NPs in the 0-50 nm range and 32.4% in 50-100 nm. FESEM (Figure 1c) illustrated surface morphology, while TEM (Figure 1d) provided internal structure details. These findings collectively confirm the effective production of well-defined ZnO-NPs via green synthesis.

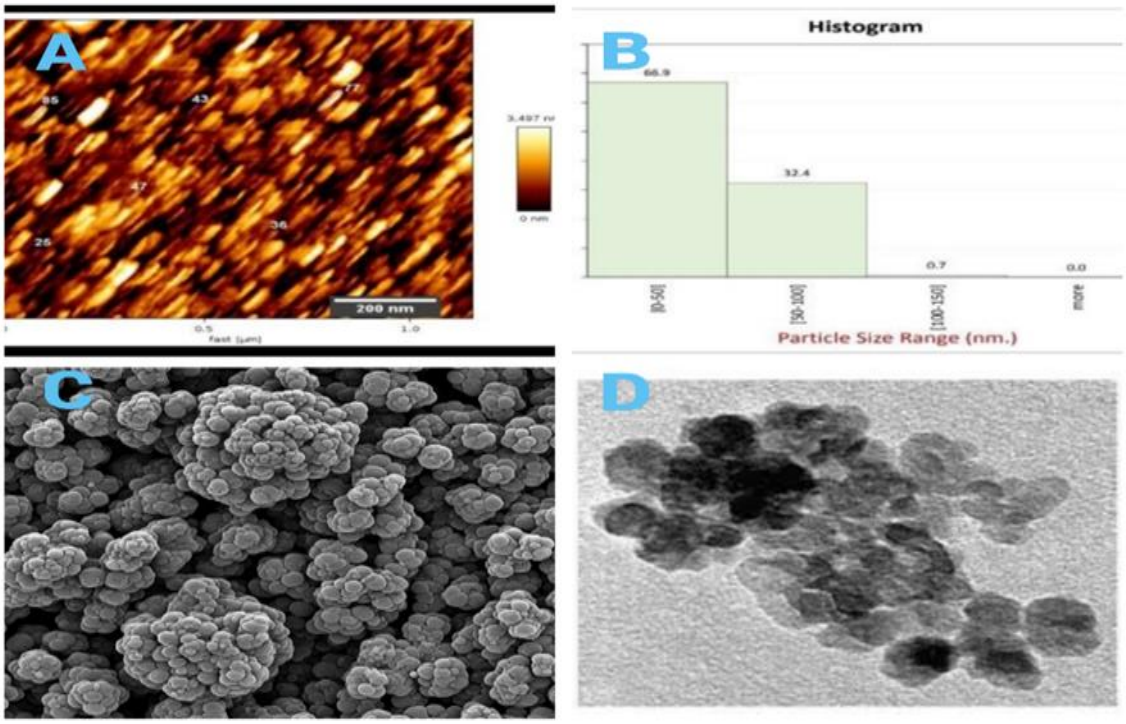


Figure 1. Comprehensive characterization of green-synthesized ZnO nanoparticles. (A) AFM (B) Histogram (C) FESEM (D) TEM.

XRD analysis

The XRD analysis was performed to confirm the crystalline nature and phase purity of the green-synthesized ZnO-NPs using a GNR instrument (Italy; Model V) operating at 40 kV and 30 mA. The resulting XRD pattern (Figure 2) exhibited well-defined and sharp diffraction peaks at approximate 2θ values of 34.5∘, 36.5∘, 39.0∘, 56.5∘, 67.0∘, 71.5∘, and 76.5∘. These peaks were successfully indexed to the (100), (002), (101), (102), (110), (103), and (220) crystallographic planes, respectively, which are characteristic of the hexagonal wurtzite structure of ZnO. The alignment of these peaks with the standard JCPDS card No. 36-1451 (as implied by the ZnO standard reference) coupled with the absence of any additional or spurious peaks, confirms the successful synthesis of highly pure, crystalline ZnO-NPs and validates the material's structural integrity.

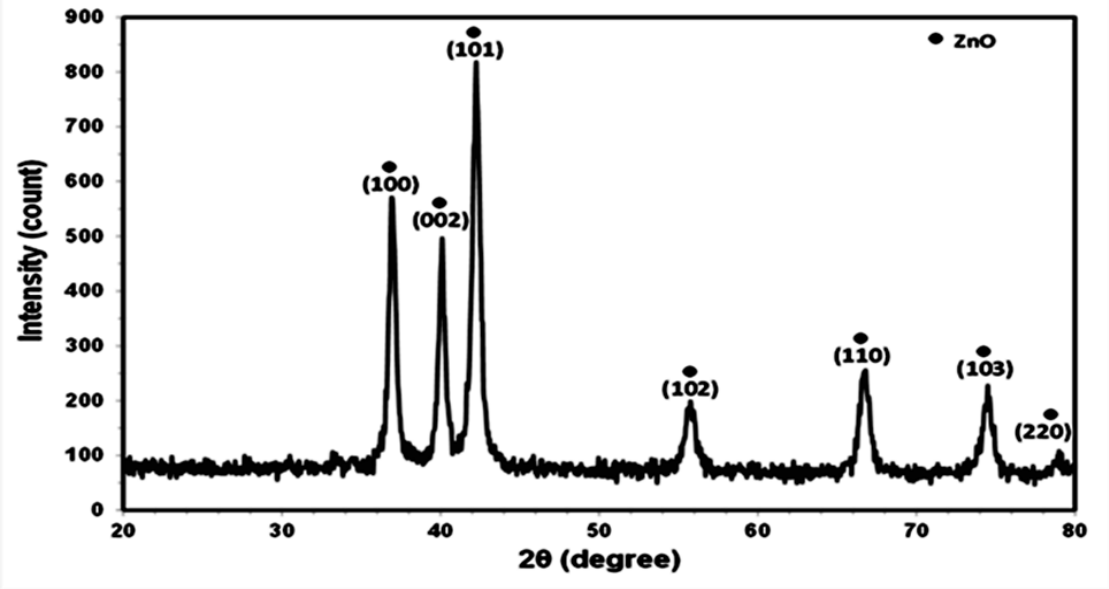


Figure 2. XRD pattern of green-synthesized ZnO-NPs

DLS analysis

DLS was performed to determine the hydrodynamic size and particle size distribution of the synthesized nanoparticles in a colloidal solution. The DLS plot (Figure 3) revealed a narrow size distribution, with a prominent peak centered at approximately 44.6 nm. This result, which is consistent with the average particle size obtained from other characterization techniques, confirms the successful synthesis of nanoparticles with high size uniformity. Furthermore, the DLS analysis complemented the other findings by verifying that 99.3% of the particles were within the nanoscale range, thereby substantiating the high efficiency of the green synthesis approach.

FTIR analysis

FTIR spectroscopy was conducted to identify the functional groups on the surface of the green-synthesized ZnO-NPs. The FTIR spectrum (Figure 4) revealed several characteristic absorption bands: a broad, strong band at 3411.77 cm^{-1} is attributed to the O-H stretching vibrations of surface hydroxyl groups from adsorbed water or residual phytochemicals. A distinct peak at 1636.99 cm−1 is primarily assigned to the bending vibration of adsorbed water (H-O-H), though it may also involve C=O stretching from organic components. Another significant band at 1121.12 cm^{-1} indicates C-O stretching vibrations, confirming the presence of organic compounds from the *P. oleracea* extract that act as capping agents. Most importantly, the strong absorption bands in the low-wavenumber region, specifically at

600.92 cm^{-1} and 448.52 cm^{-1}, are characteristic of the Zn-O stretching vibrations, providing definitive evidence for the successful formation of the ZnO-NPs. These findings collectively demonstrate the effective role of plant-derived phytochemicals in the stabilization and surface functionalization of the nanoparticles.

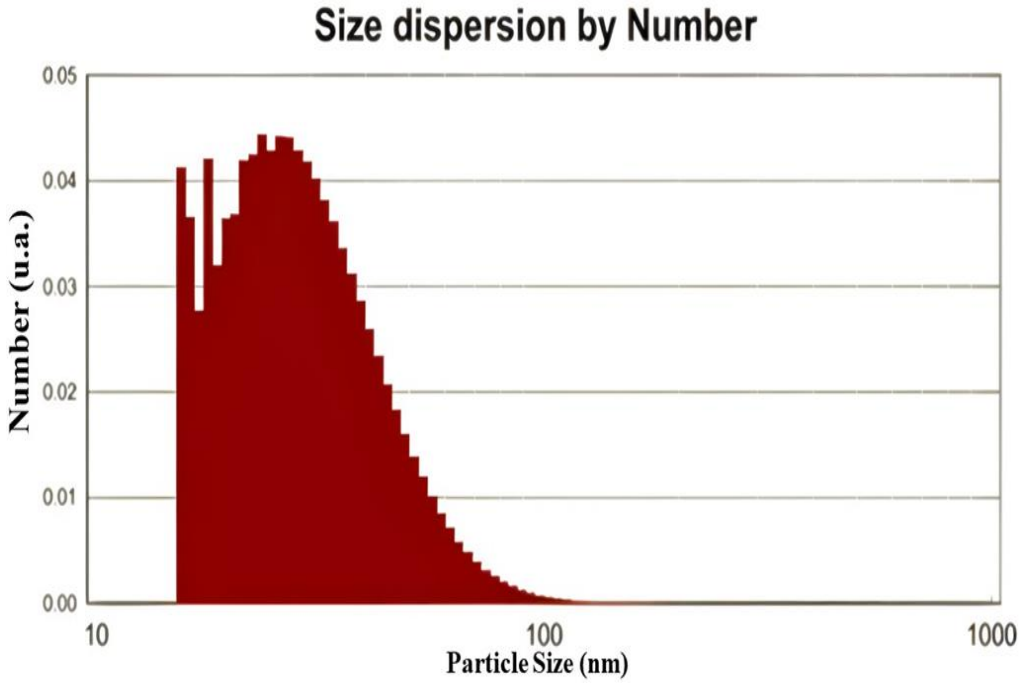


Figure 3. DLS size distribution by number of ZnO-NPs in the range of 10–1000 nm

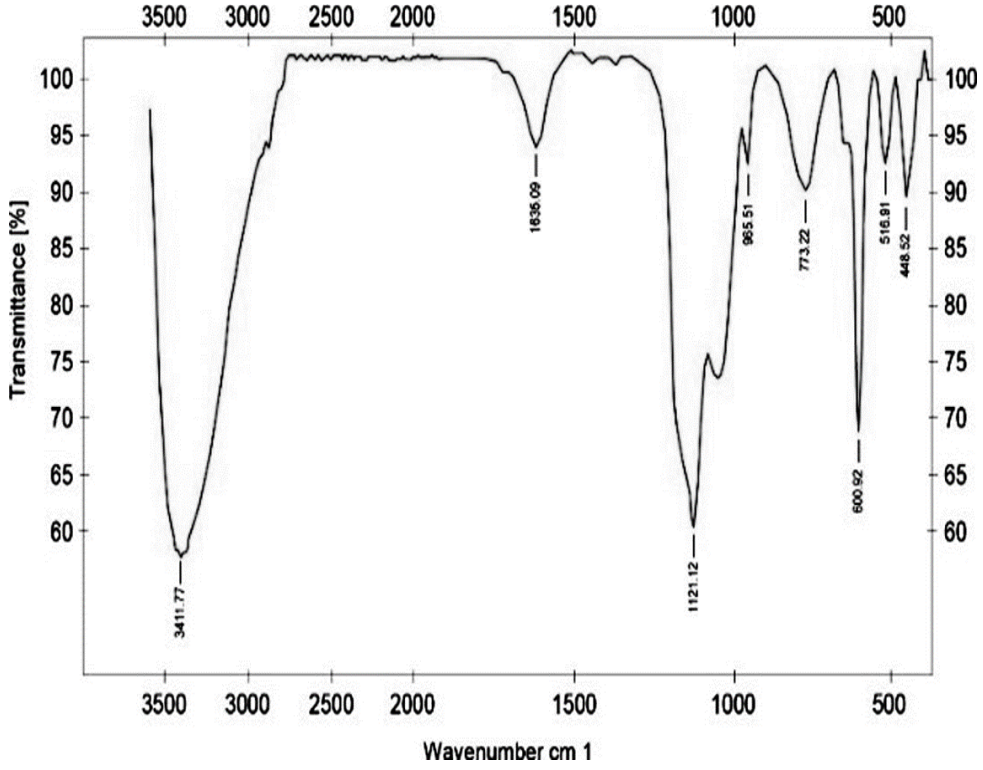


Figure 4. FTIR spectrum of green-synthesized ZnO-NPs

MTT assay

The anticancer efficacy of green-synthesized ZnO-NPs was robustly demonstrated through the MTT assay, which revealed a significant concentration- and time-dependent reduction in the viability of AGS gastric cancer cells (Figure 5). Following a 48-hr treatment period, cell viability progressively declined from 100% in the untreated control to 93.76, 89.67, 85.25, 83.18, 73.21, 57.62, and 53.79% at concentrations of 1, 2, 4, 6, 10, 15, and 20 µg/mL, respectively. This cytotoxic effect was further amplified at the 72-hr mark, with viability plummeting to 93.82, 88.15, 84.2, 77.46, 67.52, 55.26, and 41.4% at concentrations of 1, 2, 4, 6, 10, 15, and 20 µg/mL, respectively. The calculated IC50 values of 24.84 µg/mL for 48 hr and 16.88 µg/mL for 72 hr underscore this potent effect. Statistical analysis confirmed a significant difference ($p<0.05$) between all treated groups and the control. Importantly, a parallel investigation on normal HEK-293 cells revealed no significant cytotoxic effects (Figure 6), as their viability remained high (between 92.63 and 93.5% at the highest concentration) after both 48 and 72 hr. These compelling results highlight the selective and potent cytotoxic activity of ZnO-NPs, targeting cancerous AGS cells while exhibiting minimal toxicity to normal HEK-293 cells.

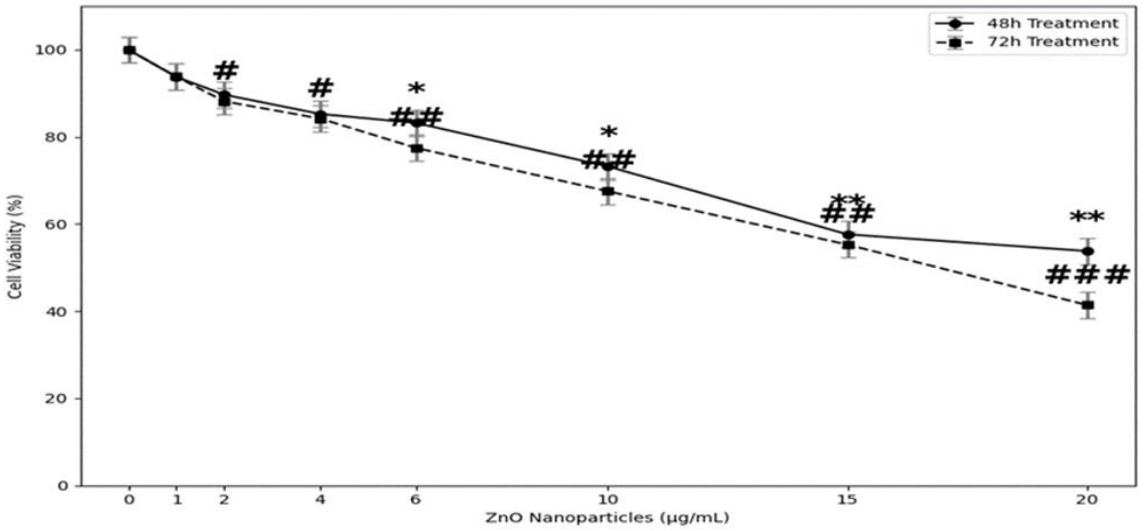


Figure 5. Cell viability of AGS cancer cells treated with green-synthesized ZnO-NPs at various concentrations and time points. Cell viability decreased with increasing concentration and treatment time. (Data are presented as mean ± SEM). ***p<0.001, **p<0.01, and *p<0.05.

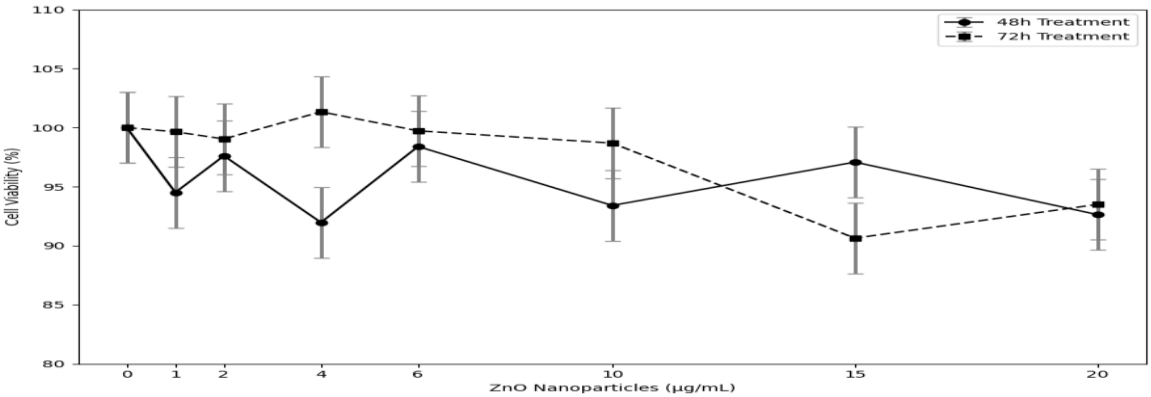


Figure 6. Effect of green-synthesized ZnO-NPs, prepared using *Portulaca oleracea* extract, on the viability of normal human embryonic kidney fibroblast (HEK-293) cells after 48 and 72 hr of treatment. ZnO-NPs showed no cytotoxic effect on the normal cell line. (Data are presented as mean ± SEM).

Annexin V-PI assay

Flow cytometry analysis confirmed that ZnO-NPs induced programmed cell death in AGS gastric cancer cells in a manner that was both time- and dose-dependent. The untreated control cell population maintained high viability at 89.9%, as seen in Figure 7A. However, exposure to the 48-hr IC50 concentration initiated a statistically significant cascade of cellular events, as shown in Figure 7B. Viable cells dropped to 60.6% ($p<0.001$), with a concurrent, significant rise in early apoptotic cells (Q3) to 14.5% ($p<0.001$) and late apoptotic/necrotic cells (Q2) to 8.03% ($p<0.01$). At this initial stage, necrotic cells (Q1) also showed a marked increase to 16.9%. The cytotoxic effect intensified by the 72-hr IC50 time point, as illustrated in Figure 7C, where the viable population further diminished to 37.0% ($p<0.001$). This decline was mirrored by a profound and statistically significant expansion of the early apoptotic population to 25.4% ($p<0.001$), while late apoptotic/necrotic cells swelled to 29.5% ($p<0.001$). Although the percentage of necrotic cells (Q1) subsided to 8.13% at this later time point, the overarching trend of apoptosis, as demonstrated by the dramatic increase in the Q2 and Q3 populations, firmly establishes it as the predominant mechanism of cell death induced by ZnO-NPs.

DAPI staining of nuclear morphology

DAPI staining served as a powerful tool to visually confirm the induction of apoptosis by ZnO-NPs in AGS gastric cancer cells, revealing a progression of distinct morphological changes (Figure 8). Untreated control cells (Figure 8A) presented with nuclei that were typically large and well-defined, displaying a uniform and diffuse chromatin distribution, a hallmark of cellular health. In stark contrast, cells exposed to ZnO-NPs at IC50 concentrations underwent a series of dramatic transformations. At the 48-hr time point (Figure 8B), a notable increase in nuclear damage was observed, characterized by the appearance of nuclear condensation (pyknosis), where nuclei appeared smaller and hyper-fluorescent, and nuclear fragmentation (karyorrhexis), wherein the nuclei had fragmented into multiple distinct pieces. By the 72-hr mark (Figure 8C), these morphological indicators of cell death were even more pervasive. The marked decline in overall cell density, coupled with the widespread prevalence of these aberrant nuclear morphologies, provides compelling visual evidence of a time-dependent induction of apoptosis. This finding corroborates the results of the flow cytometry analysis, firmly establishing apoptosis as the primary mechanism of cell death triggered by ZnO-NPs.

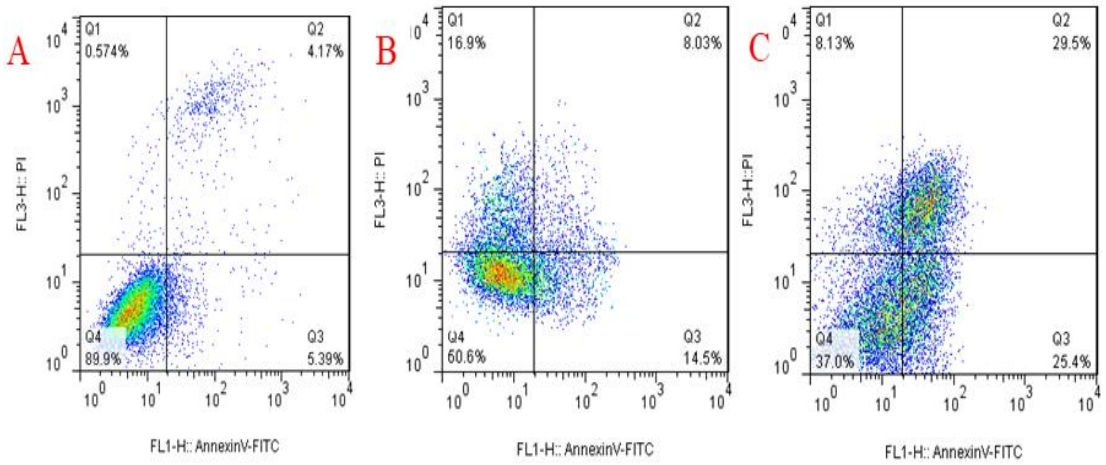


Figure 7. Representative flow cytometry plots (Annexin V-PI assay) of AGS gastric cancer cells. (A) Untreated control. (B) 48-hr IC50 ZnO NP treatment. (C) 72-hr IC50 ZnO NP treatment.

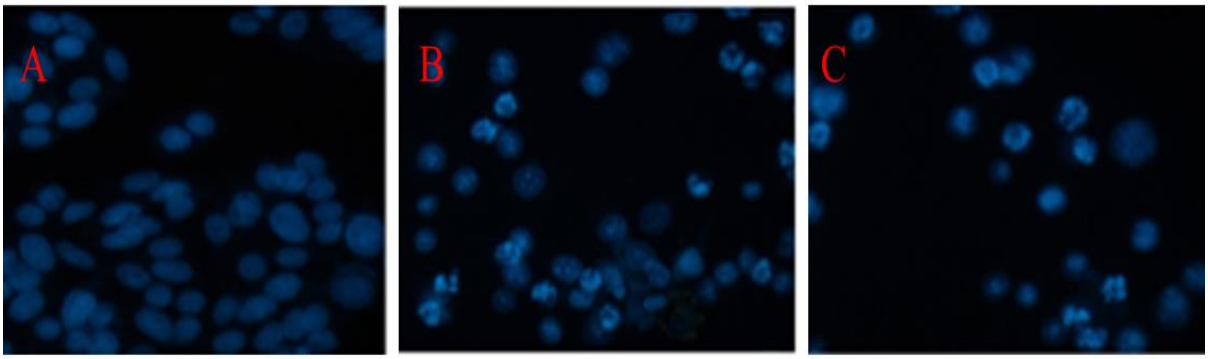


Figure 8. Representative DAPI-stained images of nuclear morphological changes in cells. (A) Untreated control. (B) 48-hr IC50 treatment. (C) 72-hr IC50 treatment.

Antioxidant test

The FRAP assay demonstrated a dose- and time-dependent increase in the extracellular antioxidant capacity of green-synthesized ZnO-NPs in AGS cell culture supernatant ($p<0.05$). Significant antioxidant activity began at 6 µg/mL after 48 hr, peaking at 20 µg/mL (Figure 9). At 72 hr, activity started at a lower concentration of 4 µg/mL, indicating enhanced potency, and similarly peaked at 20 µg/mL (Figure 10). These findings highlight robust, concentration-dependent antioxidant properties improving with prolonged exposure.

Gene expression at IC50 concentrations

Relative gene expression of key apoptotic regulators (*Bax*, *P53*, *Caspase-3*, *Caspase-9*, and *Bcl-2*) was analyzed (Figure 11 and Table 2). Pro-apoptotic genes (*Bax*, *P53*, *Caspase-3*, and *Caspase-9*) showed significant upregulation in both the 48-hr IC50 (24.84 µg/mL) and 72-hr IC50 (16.88 µg/mL) treated groups compared to the control. Conversely, the anti-apoptotic gene *Bcl-2* was significantly downregulated. Upregulation of pro-apoptotic genes appeared slightly higher at the 48-hr IC50. This modulation strongly indicates that ZnO NPs induce apoptosis by influencing the balance between these regulatory genes.

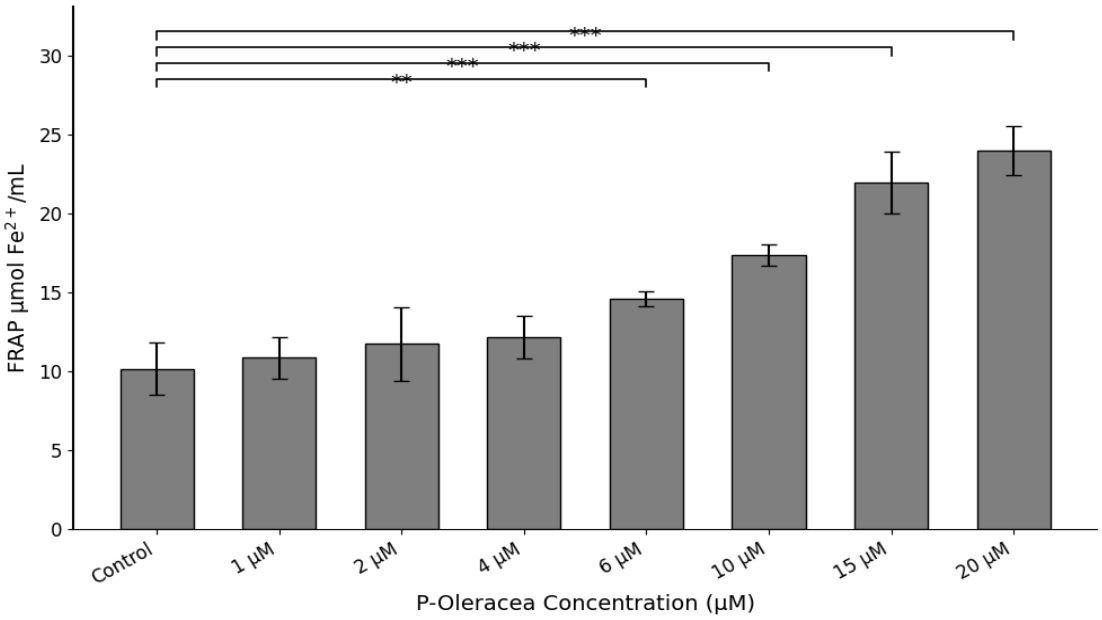


Figure 9. FRAP of green-synthesized ZnO-NPsat various concentrations after 48 hr of treatment. Data present mean ± SEM. ***$p<0.001$, **$p<0.01$, and *$p<0.05$.

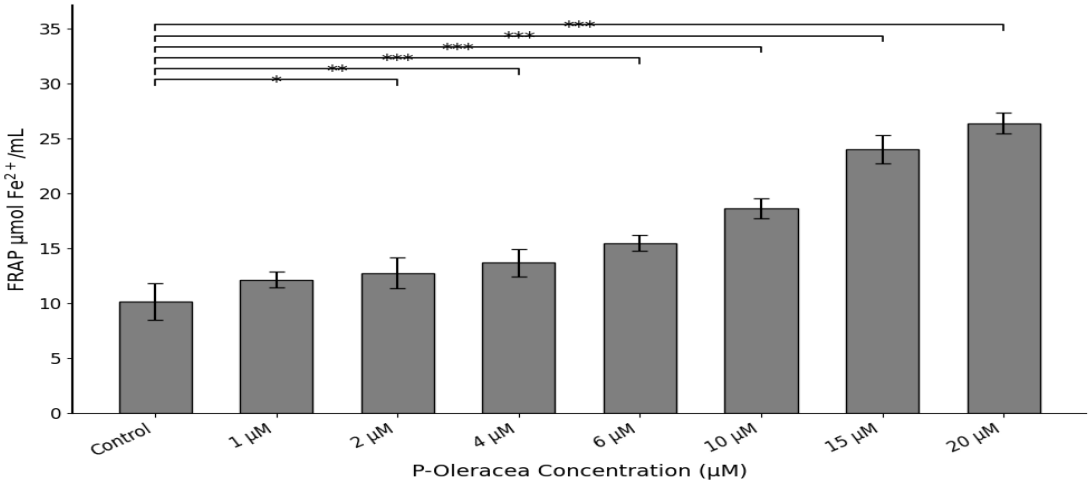


Figure 10. FRAP of green-synthesized ZnO-NPsat various concentrations after 72 hours of treatment. Data present mean ± SEM. ***p<0.001, **p<0.01, and *p<0.05.

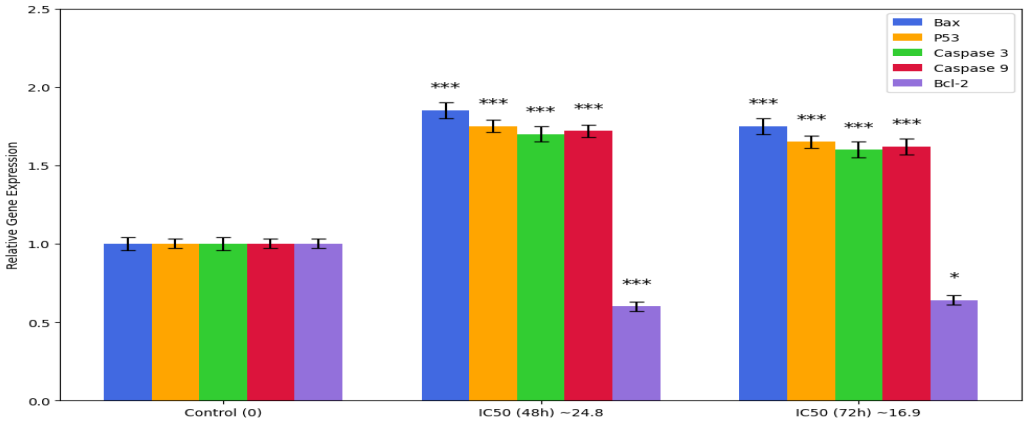


Figure 11. Comparison of apoptotic gene expression profiles at ic50 concentrations of ZnO-NPs. Data present mean ± SEM. ***p<0.001, **p<0.01, and *p<0.05.

Table 2. Relative gene expression levels (mean ± SEM) of apoptotic and anti-apoptotic genes in ZnO-NPs-treated cells

Condition	**Conc. (µg/mL)**	***Bax***	***P53***	***Caspase 3***	***Caspase 9***	***Bcl-2***
Control	0	1.00 ± 0.04	1.00 ± 0.03	1.00 ± 0.04	1.00 ± 0.03	1.00 ± 0.03
IC50 (48hr)	~24.84	1.85 ± 0.05 p=0.0008***	1.75 ± 0.04 p=0.0011***	1.70 ± 0.05 p=0.0010***	1.72 ± 0.04 p=0.0009***	0.60 ± 0.03 p=0.0025***
IC50 (72hr)	~16.88	1.75 ± 0.05 p=0.0012***	1.65 ± 0.04 p=0.0018***	1.60 ± 0.05 p=0.0020***	1.62 ± 0.05 p=0.0015***	0.64 ± 0.03 p=0.0030***

CAM analysis

CAM assay evaluated green-synthesized ZnO-NPs (400-700 µg/mL) anti-angiogenic effects in chicken eggs. On day 8, NPs were applied, and on day 12, vascular status was photographed (Figure 12). Images showed vascularization in untreated (Figure 12A) and laboratory control (Figure 12B), contrasting with treated groups (Figures 12C-F).

Effect of treatment on vascular branching

Mean vascular branching decreased dose-dependently with increasing ZnO-NP concentrations (Figure 13). Control had

~31 branches, laboratory control ~29. Treated groups showed progressive reduction: ~27 (400 µg/mL), ~24 (500 µg/mL), ~21 (600 µg/mL), and ~16 (700 µg/mL). Statistical analysis showed significantly higher branching in control vs. 500, 600, and 700 µg/mL groups, and laboratory control vs. 600 and 700 µg/mL groups. This suggests dose-dependent inhibition of vascular branching.

Effect of treatment concentration on vascular branch length

Mean vascular branch length also decreased dose-dependently (Figure 14). Control and laboratory control lengths were ~90 and ~89 units, respectively. Treated groups showed reductions: ~87 (400 µg/mL), ~79 (500 µg/mL), ~52 (600 µg/mL), and ~40 (700 µg/mL). Control showed significantly longer branches than 500, 600, and 700 µg/mL groups. The 400 µg/mL group also had significantly longer branches than 600 and 700 µg/mL groups, indicating dose-dependent inhibition of branch length.

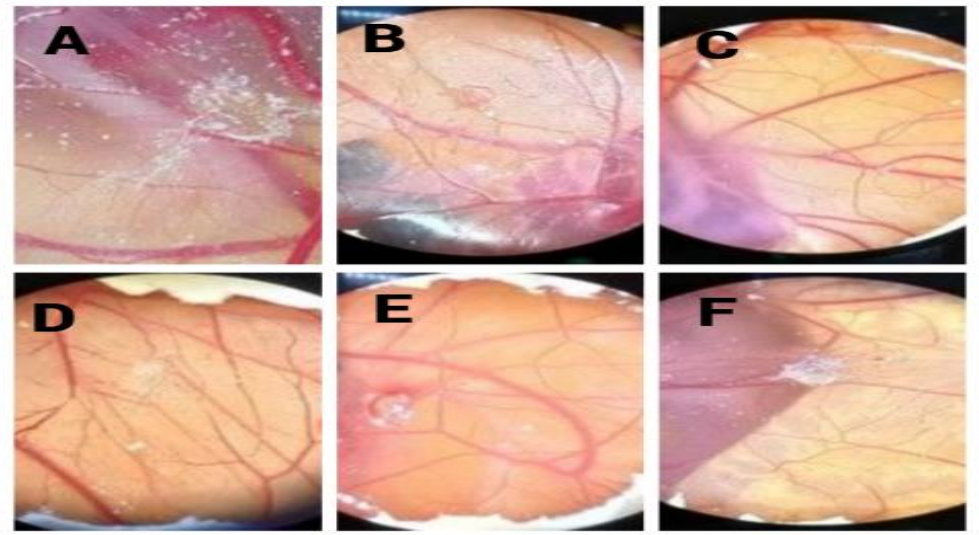


Figure 12. Stereomicroscopic images of CAM vascularization. (A) Untreated control, (B) laboratory control, and (C-F) CAMs treated with 400, 500, 600, and 700 µg/mL green-synthesized ZnO nanoparticles, respectively.

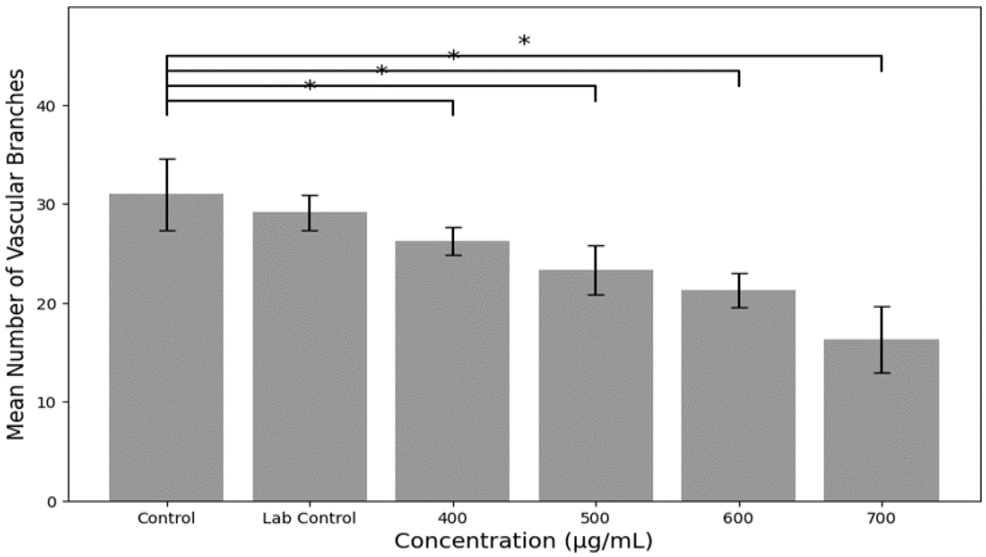


Figure 13. Mean number of vascular branches in control and various treatment groups. Asterisks indicate statistically significant differences. Data present mean ± SEM. ***p<0.001, **p<0.01, and *p<0.05.

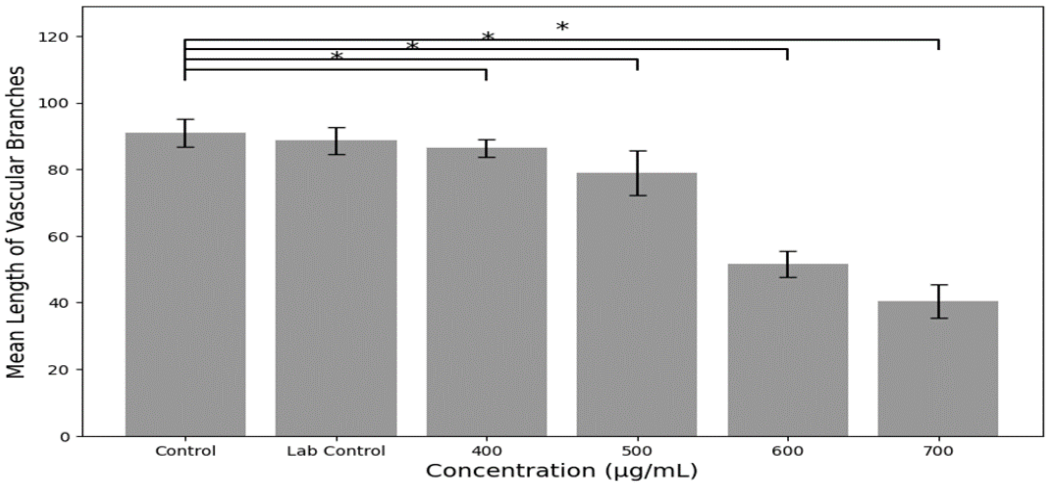


Figure 14. Mean length of vascular branches in control and various treatment concentration groups. Asterisks indicate statistically significant differences. Data present mean ± SEM. ***p<0.001, **p<0.01, and *p<0.05.

Effect of treatment concentration on mean embryo weight

Mean embryo weight decreased dose-dependently (Figure 15). Control averaged ~2.65 g, and laboratory control ~2.80 g. Treated groups showed progressive reductions: ~2.05 g (400 µg/mL), ~1.80 g (500 µg/mL), ~1.60 g (600 µg/mL), and ~1.55 g (700 µg/mL). Both control and laboratory control groups had significantly higher embryo weights than all treated groups (400, 500, 600, and 700 µg/mL), suggesting dose-dependent inhibition of embryo weight.

Effect of treatment concentration on mean Cephalo-Caudal length

Mean cephalo-caudal length also decreased dose-dependently (Figure 16). The mean length in the control group was ~34 mm, while the laboratory control group showed a comparable value. Treated groups showed reductions: ~31.5 mm (400 µg/mL), ~29.5 mm (500 µg/mL), ~28.5 mm (600 µg/mL), and ~27 mm (700 µg/mL). Control and laboratory control groups had significantly greater lengths than all treated groups (400, 500, 600, and 700 µg/mL), suggesting dose-dependent inhibition of cephalo-caudal length.

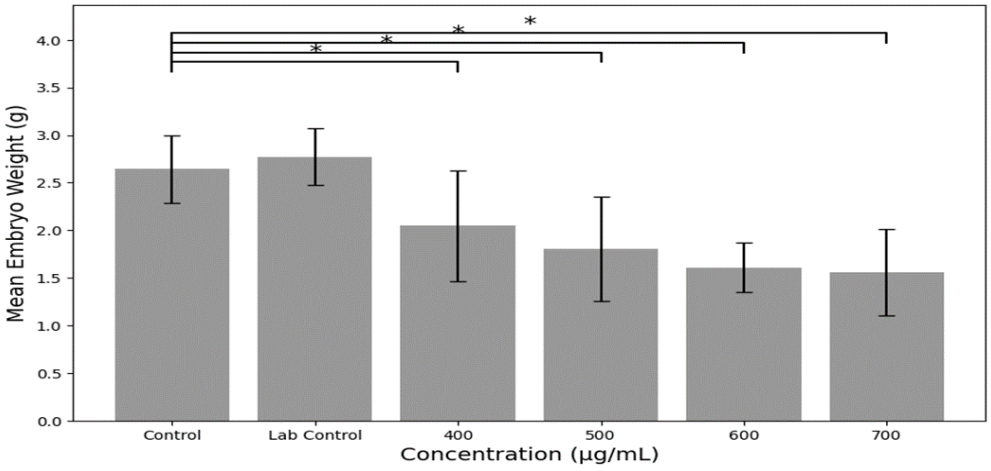


Figure 15. Mean embryo weight in control and various treatment concentration groups. Asterisks indicate statistically significant differences. Data present mean ± SEM. ***p<0.001, **p<0.01, and *p<0.05.

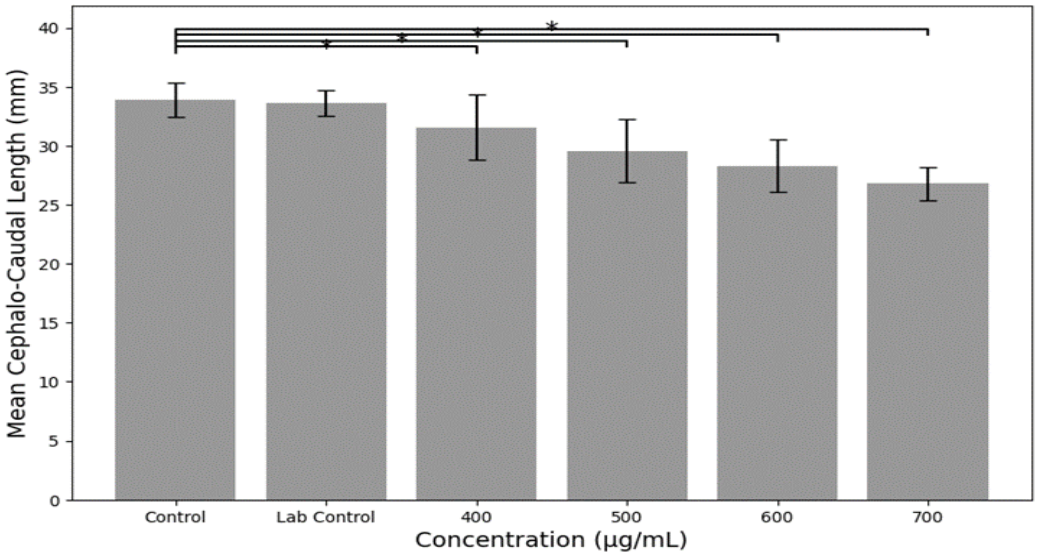


Figure 16. Mean cephalo-caudal length in control and various treatment concentration groups. Asterisks indicate statistically significant differences. Data present mean ± SEM. ***p<0.001, **p<0.01, and *p<0.05.

Discussion

This study investigated green-synthesized ZnO NPs from *P. oleracea* extract, characterizing them and assessing their multifaceted anticancer activities. Our findings consistently align with existing literature, offering insights into their implications and potential molecular mechanisms.

Our characterization confirmed successful green synthesis of crystalline ZnO NPs with nanoscale dimensions. This outcome, with particles predominantly within the nanoscale range, is consistent with extensive literature on plant-mediated metallic nanoparticle synthesis (Paramasivam et al. 2021; Radulescu et al. 2023). *Portulaca oleracea*'s rich phytochemicals (flavonoids aaand polyphenols) likely acted as reducing and capping agents, influencing particle properties, a mechanism supported by studies demonstrating how plant metabolites dictate nanoparticle characteristics (Elhabal et al. 2024). This green approach offers significant environmental advantages over traditional methods, supporting sustainable nanotechnological production (Verma et al. 2019). The demonstrated efficiency and sustainability of this method highlight its potential for scalable and environmentally benign nanoparticle production.

Our cytotoxicity studies on AGS gastric cancer cells revealed a significant concentration- and time-dependent reduction in cell viability, aligning with numerous reports on ZnO NP anticancer potential across various cancer lines (Sharma et al. 2020; Hussien et al. 2025). The primary mechanism is widely attributed to reactive oxygen species (ROS) generation, leading to oxidative stress and cellular dysfunction (Li et al. 2021). Crucially, we observed selective toxicity, with no significant adverse effects on normal HEK-293 cells. This differential sensitivity is a key advantage in nanomedicine, as cancer cells are often more vulnerable to oxidative burden due. This finding supports the development of these green-synthesized ZnO NPs as targeted anticancer agents with reduced systemic toxicity.

Our mechanistic studies clearly indicated that ZnO NPs primarily induce apoptosis (Ma and Yang 2016), evidenced by morphological changes like nuclear condensation/fragmentation and distinct apoptotic cell populations via Annexin V-

PI staining (Anjum et al. 2021). Gene expression analysis further confirmed this: significant upregulation of pro-apoptotic genes (*Bax, P53, Caspase-3, and Caspase-9*) and downregulation of anti-apoptotic *Bcl-2* (El-Saadony et al. 2024). This modulation of the *Bax*/*Bcl-2* ratio favors mitochondrial outer membrane permeabilization (MOMP), releasing pro-apoptotic factors that activate initiator *Caspase-9*, leading to effector *Caspase-3* activation and apoptotic demise (Xie et al. 2023). Upregulation of *P53* further suggests its role in enhancing pro-apoptotic gene expression (Aldalbahi et al. 2020). These molecular findings align with studies detailing mitochondrial apoptotic pathway and *P53*-dependent mechanisms in ZnO NP-induced cell death (Sharma et al. 2020; Anjum et al. 2021). Our data predominantly points to the intrinsic pathway as the primary mechanism.

Interestingly, our FRAP assay showed extracellular antioxidant capacity for green-synthesized ZnO NPs, with dose- and time-dependent increases. While their pro-oxidant properties inside cancer cells drive cytotoxicity, this extracellular antioxidant activity adds complexity. This duality is consistent with context-dependent nanoparticle behavior, where some metallic NPs can scavenge free radicals, especially extracellularly (Sirelkhatim et al. 2015). Other metal oxide NPs also show antioxidant properties via mechanisms like superoxide dismutase (SOD) mimicry or direct radical quenching (Mutukwa et al. 2022; Mongy and Shalaby 2024). This suggests that ZnO NPs might interact sophisticatedly with redox balance, potentially contributing to biocompatibility or influencing tumor microenvironment redox signaling.

Based on the CAM assay, the green-synthesized ZnO NPs demonstrated robust anti-angiogenic properties, a critical therapeutic advantage for cancer treatment (Bogdan et al. 2017). Our findings revealed a clear dose-dependent inhibition of both vascular branching and length, which was further evidenced by a significant reduction in embryo development. This aligns with a growing body of literature highlighting the potential of various nanoparticles, including ZnO NPs, as inhibitors of tumor vascularization (Bisht and Rayamajhi 2016). The anti-angiogenic effects of ZnO NPs are due to their ability to disrupt key molecular pathways essential for new blood vessel formation. Our study confirms that these NPs interfere with endothelial cell function, including their proliferation, migration, and tube formation (Wahab et al. 2014). Specifically, the ZnO NPs regulate crucial signaling pathways, such as vascular endothelial growth factor (VEGF) signaling, and alter the activity of matrix metalloproteinases (MMPs), which are vital for extracellular matrix remodeling during angiogenesis (Cabral-Pacheco et al. 2020). The capacity of our green-synthesized ZnO NPs to disrupt tumor blood supply suggests a powerful, multi-pronged therapeutic approach, which not only directly induces cancer cell death but also starves the tumor by limiting the resources required for its growth and metastasis.

Due to resource and funding constraints, the Annexin V-FITC/PI flow cytometry experiments were conducted once per treatment condition, without biological or technical replicates. While meticulous care was taken to ensure accuracy throughout all stages, this constitutes a significant methodological limitation. This is particularly relevant for the CAM assay, where inherent variability in chick embryo development may influence the outcomes. Despite the clear and statistically significant differences observed between treated and control groups, this limitation potentially reduces the statistical power and generalizability of the results. Therefore, future studies are recommended to include increased numbers of biological and technical replicates to strengthen the statistical evidence and the validity of the findings. Additionally, due to financial constraints, in vivo experiments were not feasible within

the scope of this study; such investigations are essential in future research to comprehensively evaluate the safety and clinical efficacy of ZnO NPs.

This study successfully demonstrated the green synthesis of well-characterized ZnO NPs from *P. oleracea* extract. These NPs exhibited selective anticancer activity against AGS gastric cancer cells, primarily by inducing apoptosis through the modulation of key apoptotic genes. Furthermore, the ZnO NPs displayed significant anti-angiogenic properties in the CAM assay, inhibiting vascular branching and length, and impacting embryo development in a dose-dependent manner. While also showing extracellular antioxidant capacity, these findings collectively highlight the promising multi-modal therapeutic potential of green-synthesized ZnO NPs as an effective agent for both directly targeting cancer cells and inhibiting tumor vascularization.

Acknowledgment

The authors gratefully acknowledge the Organization of Libraries, Museums and Document Center of Astan Quds Razavi for their invaluable support and provision of relevant informational resources, which significantly contributed to the successful completion of this study. Furthermore, sincere appreciation is extended to all individuals who rendered assistance during the course of this research endeavor.

Conflicts of interest

The authors declare that they have no competing interests.

Funding

This research received financial backing from the Club of Young Researchers and Elites in Mashhad, Iran, under grant number 4023598.

Ethical Considerations

The study received ethical approval from the Islamic Azad University, Mashhad Branch Research Ethics Committee, under the ethical code IR.IAU.MSHD.REC.1402.159. All experimental procedures involving fertilized chicken eggs were conducted in accordance with the relevant institutional and national guidelines for the care and use of animals in research.

Code of Ethics

IR.IAU.MSHD.REC.1402.159.

Authors' Contributions

MP was crucial for sample collection, test execution, and methodology development, and also took charge of data curation, validation, and performed statistical analysis. MP prepared the final manuscript. FF provided assistance with sample collection and contributed to writing the manuscript. JKH and SZ were instrumental in the study's conception and experimental design. FF specifically focused on reviewing and refining the written material.

Abbreviations

AFM: Atomic Force Microscopy
Bax: Bcl-2-Associated X Protein
Bcl-2: B-cell Lymphoma 2
CAM: Chorioallantoic Membrane
DAPI: 4′,6-Diamidino-2-Phenylindole
DLS: Dynamic Light Scattering
FESEM: Field Emission Scanning Electron Microscopy
FRAP: Ferric Reducing Antioxidant Power
FTIR: Fourier-Transform Infrared Spectroscopy
IC50: Half-Maximal Inhibitory Concentration
ROS: Reactive Oxygen Species
SEM: Standard Error of the Mean
TAS: Total Antioxidant Status
TEM: Transmission Electron Microscopy
VEGF: Vascular Endothelial Growth Factor
XRD: X-ray Diffraction

References

Acebes-Fernández, V., Landeria-Viñuela, A., Juanes-Velasco, P., Hernández, A. P., Otazo-Perez, A., Manzano-Román, R., Gongora, R., & Fuentes, M. (2020). Nanomedicine and Onco-Immunotherapy: From the Bench to Bedside to Biomarkers. Nanomaterials (Basel), 10(7), 1274.

Aldalbahi, A., Alterary, S., Ali Abdullrahman Almoghim, R., Awad, M. A., Aldosari, N. S., Fahad Alghannam, S., Nasser Alabdan, A., Alharbi, S., Ali Mohammed Alateeq, B., Abdulrahman Al Mohsen, A., Alkathiri, M. A., & Abdulrahman Alrashed, R. (2020). Greener Synthesis of Zinc Oxide Nanoparticles: Characterization and Multifaceted Applications. Molecules, 25(18), 4198.

Alshiraihi, I., & Kato, T. A. (2023). Apoptosis Detection Assays. Methods Mol Biol, 2519, 53–63.

Anjum, S., Hashim, M., Malik, S. A., Khan, M., Lorenzo, J. M., Abbasi, B. H., & Hano, C. (2021). Recent Advances in Zinc Oxide Nanoparticles (ZnO NPs) for Cancer Diagnosis, Target Drug Delivery, and Treatment. Cancers (Basel), 13(18), 4570.

Bisht, G., & Rayamajhi, S. (2016). ZnO Nanoparticles: A Promising Anticancer Agent. Nanobiomedicine (Rij), 3, 9.

Bogdan, J., Pławińska-Czarnak, J., & Zarzyńska, J. (2017). Nanoparticles of Titanium and Zinc Oxides as Novel Agents in Tumor Treatment: A Review. Nanoscale Res Lett, 12(1), 225.

Bustin, S. A., Benes, V., Garson, J. A., Hellemans, J., Huggett, J., Kubista, M., Mueller, R., Nolan, T., Pfaffl, M. W., Shipley, G. L., Vandesompele, J., & Wittwer, C. T. (2009). The MIQE guidelines: Minimum information for publication of quantitative real-time PCR experiments. Clin Chem, 55(4), 611–622.

8. Cabral-Pacheco, G. A., Garza-Veloz, I., Castruita-De la Rosa, C., Ramirez-Acuña, J. M., Perez-Romero, B. A., Guerrero-Rodriguez, J. F., Martinez-Avila, N., & Martinez-Fierro, M. L. (2020). The roles of matrix metalloproteinases and their inhibitors in human diseases. Int J Mol Sci, 21(24), 9739.

Eker, F., Akdaşçi, E., Duman, H., Bechelany, M., & Karav, S. (2025). Green Synthesis of Silver Nanoparticles Using Plant Extracts: A Comprehensive Review of Physicochemical Properties and Multifunctional Applications. Int J Mol Sci, 26(13), 6222.

Elhabal, S. F., Abdelaal, N., Saeed Al-Zuhairy, S. A. K., Elrefai, M. F. M., Elsaid Hamdan, A. M., Khalifa, M. M., Hababeh, S., Khasawneh, M. A., Khamis, G. M., Nelson, J., Mohie, P. M., Gad, R. A., Rizk, A., Kabil, S. L., El-Ashery, M. K., Jasti, B. R., Elzohairy, N. A., Elnawawy, T., Hassan, F. E., & El-Nabarawi, M. A. (2024). Green Synthesis of Zinc Oxide Nanoparticles from Althaea officinalis Flower Extract Coated with Chitosan for Potential Healing Effects on Diabetic Wounds by Inhibiting TNF-α and IL-6/IL-1β Signaling Pathways. Int J Nanomedicine, 19, 3045–3070.

El-Saadony, M. T., Fang, G., Yan, S., Alkafaas, S. S., El Nasharty, M. A., Khedr, S. A., Hussien, A. M., Ghosh, S., Dladla, M., Elkafas, S. S., Ibrahim, E. H., Salem, H. M., Mosa, W. F. A., Ahmed, A. E., Mohammed, D. M., Korma, S. A., El-Tarabily, M. K., Saad, A. M., El-Tarabily, K. A., & AbuQamar, S. F. (2024). Green Synthesis of Zinc Oxide Nanoparticles: Preparation, Characterization, and Biomedical Applications – A Review. Int J Nanomedicine, 19, 12889–12937.

Golzar, M., Saghi, E., Rakhshandeh, H., Dehnavi, Z., Jafarzadeh Esfehani, A., & Nematy, M. (2023). Evaluating the effect of an Iranian traditional medicine-based herbal candy on body composition and appetite in overweight and obese adults: A preliminary study. Avicenna J Phytomed, 13(2), 165–176.

Haider, T., Pandey, V., Banjare, N., Gupta, P. N., & Soni, V. (2020). Drug resistance in cancer: Mechanisms and tackling strategies. Pharmacol Rep, 72(5), 1125–1151.

Hosseinpour, L., Baharara, J., Darroudi, M., Sabouri, Z., Haji Ghasem Kashani, M., & Zaker Bostanabad, S. (2025). Green synthesis of selenium nanoparticles using Cordia myxa extract and assessment of their cytotoxic and antioxidant properties. Avicenna J Phytomed, 15(5), 1531–1545.

Hussien, N. A., Khalil, M. A. E. F., Schagerl, M., & Ali, S. S. (2025). Green Synthesis of Zinc Oxide Nanoparticles as a Promising Nanomedicine Approach for Anticancer, Antibacterial, and Anti-Inflammatory

Therapies. Int J Nanomedicine, 20, 4299–4317.

Khan, F., Shariq, M., Asif, M., Siddiqui, M. A., Malan, P., & Ahmad, F. (2022). Green Nanotechnology: Plant-Mediated Nanoparticle Synthesis and Application. Nanomaterials (Basel), 12(4), 673.

Li, Y., Yang, J., & Sun, X. (2021). Reactive Oxygen Species-Based Nanomaterials for Cancer Therapy. Front Chem, 9, 650587.

Ma, D. D., & Yang, W. X. (2016). Engineered nanoparticles induce cell apoptosis: Potential for cancer therapy. Oncotarget, 7(26), 40882–40903.

Mandal, A. K., Katuwal, S., Tettey, F., Gupta, A., Bhattarai, S., Jaisi, S., Bhandari, D. P., Shah, A. K., Bhattarai, N., & Parajuli, N. (2022). Current Research on Zinc Oxide Nanoparticles: Synthesis, Characterization, and Biomedical Applications. Nanomaterials (Basel), 12(17), 3066.

Menemenli, N. Ş., Özcan, Ö., Hüsnügil, H. H., Güleç Taşkıran, A. E., Oral, G., Akyol, A., & Banerjee, S. (2025). The Chorioallantoic Membrane (CAM) Assay for the Analysis of Starvation-Induced Autophagy. Methods Mol Biol, 2879, 93–111.

Mishra, P. K., Mishra, H., Ekielski, A., Talegaonkar, S., & Vaidya, B. (2017). Zinc oxide nanoparticles: A promising nanomaterial for biomedical applications. Drug Discov Today, 22(12), 1825–1834.

Mongy, M. M., & Shalaby, M. (2024). Green synthesis of metal oxide nanoparticles and their antioxidant properties: A review. J Environ Chem Eng, 12(3), 112000.

Mongy, Y., & Shalaby, T. (2024). Green synthesis of zinc oxide nanoparticles using Rhus coriaria extract and their anticancer activity against triple-negative breast cancer cells. Sci Rep, 14(1), 13470.

Mutukwa, D., Taziwa, R., & Khotseng, L. E. (2022). A Review of the Green Synthesis of ZnO Nanoparticles Utilising Southern African Indigenous Medicinal Plants. Nanomaterials (Basel), 12(19), 3456.

Paramasivam, G., Palem, V. V., Sundaram, T., Sundaram, V., Kishore, S. C., & Bellucci, S. (2021). Nanomaterials: Synthesis and Applications in Theranostics. Nanomaterials (Basel), 11(12), 3228.

Radulescu, D. M., Surdu, V. A., Ficai, A., Ficai, D., Grumezescu, A. M., & Andronescu, E. (2023). Green Synthesis of Metal and Metal Oxide Nanoparticles: A Review of the Principles and Biomedical Applications. Int J Mol Sci, 24(20), 15397.

Rasli, N. I., Basri, H., & Harun, Z. (2020). Zinc oxide from aloe vera extract: Two-level factorial screening of biosynthesis parameters. Heliyon, 6(1), e03156.

Rauf, S., Hameed, H., Tariq, M., Afareen, A., Gulfaraz, S., AlKubaisi, N. A., & Elshikh, M. S. (2025). Phytochemical-Mediated Synthesis and Characterization of Silver Nanoparticles Using Mirabilis jalapa Leaf Extract and Their Antibacterial. Microsc Res Tech, 88(6), 1795–1805.

Sharma, P., Garg, R., & Kumari, A. (2020). A review on biogenic synthesis, applications and toxicity aspects of zinc oxide nanoparticles. EXCLI J, 19, 1325–1340.

Singh, H., Desimone, M. F., Pandya, S., Jasani, S., George, N., Adnan, M., Aldarhami, A., Bazaid, A. S., & Alderhami, S. A. (2023). Revisiting the Green Synthesis of Nanoparticles: Uncovering Influences of Plant Extracts as Reducing Agents for Enhanced Synthesis Efficiency and Its Biomedical Applications. Int J Nanomedicine, 18, 4727–4750.

Sirelkhatim, A., Mahmud, S., Seeni, A., Kaus, N. H. M., Ann, L. C., Bakhori, S. K. M., Hasan, H., & Mohamad, D. (2015). Review on Zinc Oxide Nanoparticles: Antibacterial Activity and Toxicity Mechanism. Nanomicro Lett, 7(3), 219–242.

Sung, H., Ferlay, J., Siegel, R. L., Laversanne, M., Soerjomataram, I., Jemal, A., & Bray, F. (2021). Global Cancer Statistics 2020: GLOBOCAN Estimates of Incidence and Mortality Worldwide for 36 Cancers in 185 Countries. CA Cancer J Clin, 71(3), 209–249.

Verma, A., Gautam, S. P., Bansal, K. K., Prabhakar, N., & Rosenholm, J. M. (2019). Green Nanotechnology: Advancement in Phytoformulation Research. Medicines (Basel), 6(1), 39.

Wahab, R., Siddiqui, M. A., Saquib, Q., Dwivedi, S., Ahmad, J., Musarrat, J., Al-Khedhairy, A. A., & Shin, H. S. (2014). ZnO nanoparticles induced oxidative stress and apoptosis in HepG2 and MCF-7 cancer cells and their antibacterial activity. Colloids Surf B Biointerfaces, 117, 267–276.

Wang, X., Wang, Y., Chen, Z. G., & Shin, D. M. (2009). Advances of cancer therapy by nanotechnology. Cancer Res Treat, 41(1),

1–11.
Weiskirchen, S., Schröder, S. K., Buhl, E. M., & Weiskirchen, R. (2023). A Beginner's Guide to Cell Culture: Practical Advice for Preventing Needless Problems. Cells, 12(5), 682.
Wiertelak-Makała, K., Szymczak-Pajor, I., Bociong, K., & Śliwińska, A. (2023). Considerations about Cytotoxicity of Resin-Based Composite Dental Materials: A Systematic Review. Int J Mol Sci, 25(1), 152.
Xia, L., Yang, M., & Liu, Y. (2024). Portulaca oleracea L. polysaccharide inhibits ovarian cancer via inducing ACSL4-dependent ferroptosis. Aging (Albany NY), 16(6), 5108–5122.
Xie, J., Li, H., Zhang, T., Song, B., Wang, X., & Gu, Z. (2023). Recent Advances in ZnO Nanomaterial-Mediated Biological Applications and Action Mechanisms. Nanomaterials (Basel), 13(9), 1500.